Tunable structural, morphological and optical properties of undoped, Mn, Ni and Ag-doped CuInS2 thin films prepared by AACVD

DOI:
10.1016/j.mssp.2021.106224

Document Version
Accepted author manuscript

Tunable Structural, Morphological and Optical Properties of Undoped, Mn, Ni and Ag-doped $CuInS_2$ Thin Films Prepared by AACVD

[a]Shanna-Kay Ming, [*a]Richard A. Taylor, [b,c]Paul O'Brien, [b]Paul D. McNaughter and [c]David J. Lewis

[a]Department of Chemistry, The University of the West Indies, St. Augustine, Trinidad and Tobago.
*Email: richard.taylor@sta.uwi.edu
[b]Department of Chemistry, The University of Manchester, UK.
[c]Department of Materials, The University of Manchester, UK.

Abstract

The preparation of high-quality copper indium sulphide, $CuInS_2$ photo-absorber material with tunable properties for efficient, low-cost, thin film solar cells using scalable methods remains a challenge. In order to address this, high quality off-stoichiometric undoped and Mn, Ni and Ag-doped $CuInS_2$ (CIS) thin films have been deposited onto glass substrates by aerosol-assisted chemical vapour deposition (AACVD) using metal diethyldithiocarbamate precursors at temperatures of 350, 400 and 450 °C. Data from powder X-ray diffraction (p-XRD), Raman spectroscopy and scanning electron microscopy-energy dispersive X-ray spectroscopy (SEM-EDS) suggest a correlation of morphology and composition of tetragonal phase (chalcopyrite and copper-gold-type) sulphur-deficient microcrystalline CIS thin films. For undoped thin films, near-infrared optical absorption and emission with tunable band gap between 1.32 and 1.42 eV are likely associated with donor-acceptor pairs involving deep or shallow electronic states such as sulphur vacancies ($V_S^{\bullet\bullet}$), indium-copper anti-sites ($In_{Cu}^{\bullet\bullet}$) and indium interstitials ($In_i^{\bullet\bullet\bullet}$) as donors and copper vacancies (V_{Cu}') as acceptors. Whilst Mn-doped thin films exhibit minimal tunable properties, Ni and Ag-doped films exhibit tunable morphology, composition and near-infrared absorption for small dopant content. Though further studies are required to explore the defect chemistry, these results show the utility of AACVD in tuning structural, morphological and optical properties of undoped, Mn, Ni and Ag-doped CIS thin films.

Keywords: copper indium sulphide, AACVD, doped thin films, tunable optical properties, photovoltaic material.

Introduction

Copper indium disulphide, $CuInS_2$ (CIS), is a promising ternary I-III-VI_2 chalcogenide semiconductor absorber material for thin film photovoltaics (PVs) because of its high absorption coefficient (~10^5 cm^{-1}), excellent photostability and direct band gap of ~1.5 eV (bulk) which matches well with the AM 1.5 solar emission spectrum.[1,2] Though theoretical conversion efficiencies are 27 – 32 % for CIS based solar cells, practical efficiencies are ~13 %, attributed to charge carrier recombination losses.[2] Notably, the properties and utility of CIS are comparable to those of the more widely studied quaternary $Cu(In,Ga)Se_2$ (CIGSe) or $Cu(In,Ga)(S,Se)_2$ (CIGSSe) compounds,[3] due to different preparation methods and cell architectures that maximize cell efficiency and lower production costs.[4] Notably, the chalcopyrite structure of CIS can tolerate defects from a large range of anion and cation off-stoichiometry.[5-8] Controlling these intrinsic defects can result in n or p-type conductivities, and this along with tuning optical properties,[9] film morphology and homogeneity are important pursuits.[10] However, in light of the interest over the last decade into tunable optoelectronic properties of doped chalcogenides,[5,11,12] the paucity of reports on doped CIS is noteworthy. For example, PV cells with Ti-doped CIS exhibited improved open circuit voltages and increased efficiency whilst Al-doped CIS exhibited higher absorptivity.[13] Cells with Zn and Mg-doped CIS had low photocurrents at high dopant concentrations, however with very small amounts, open circuit voltages improved,[3,13] and Klenk *et al*. demonstrated that Ga-doped CIS improved cell efficiencies.[3] These outcomes demonstrate the potential of doped CIS to influence and improve the performance characteristics of solar cells.

Notwithstanding the attractive features of CIS, controlled deposition of high quality thin films remains a challenge, and this along with insufficiency of scalable cost-effective deposition methods are obstacles toward commercialization of CIS based solar cells. Of the variety of deposition methods available, aerosol-assisted chemical vapour deposition (AACVD), the advantages of which have been reported[2,14-18] has the potential to address the synthetic challenge. Nonetheless, there are several reports highlighting challenges with depositing high quality thin films using CVD, metal-organic chemical vapor deposition (MOCVD), low-pressure-MOCVD and AACVD.[18-21] In these, thin films were deposited from various molecular precursors, for example asymmetrical dialkyldithiocarbamates,[19] bis(ethylisobutylacetates), tris(*N*,*N*-ethylbutyldithiocarbamates)[21] and single-source precursors such as $[Bu_2In\text{-}(SiPr)Cu(S_2CNiPr_2)]$[20] and $[(PPh_3)_2Cu(SEt)_2In(SEt)_2]$.[18] Typically, films were non-stoichiometric, polyphasic (e.g. either $CuInS_2$ with $CuIn_5S_8$ or $CuInS_2$

with In_6S_7),[20] inhomogeneous, of variable morphology and consisted of binary phase impurities (CuS_x, *b*-In_2S_3)[19] suggesting that film quality is dependent on precursor decomposition, nucleation and particle growth mechanisms. Furthermore, use of single-source precursors though attractive presents limitations since they are difficult to synthesize especially with dopant ions incorporated. However, more judicious approaches can be employed to controllably tune the structural and optical properties of CIS thin films using AACVD considering its versatility. Therefore, with the ability to access a range of soluble molecular precursors *via* AACVD and the potential to tune optoelectronic properties of CIS with metal ion dopants, we report for the first time, high quality, phase pure undoped, Mn^{2+}, Ni^{2+} and Ag^{+}-doped CIS thin films deposited onto glass substrates using the facile, straightforward, non-vacuum and scalable AACVD method at moderate temperatures from easily synthesized, air stable and environmentally benign metal diethyldithiocarbamate precursors. We demonstrate versatility of these precursors in combination under precise conditions to effectively control phase purity, stoichiometry, film homogeneity, morphology and tune optical properties.

Results and discussion

A. Undoped CIS films

Structural characterization

Normalized powder X-ray diffractograms for films deposited at temperatures of 350, 400 and 450 °C for 30 and 60 minutes respectively, and at 400 °C for 240 minutes in Figure 1 show characteristic reflections confirming the tetragonal chalcopyrite (CH) structure (ICDD reference no. 00-027-0159).[22] Absence of peaks associated with binary phases, copper or indium sulphide suggests a single phase. It is observed that longer deposition time and higher temperature result in more compact, crystalline films as seen from increased intensity of the primary reflections recorded in Table S1 ESI†. The exception to this is the (112) reflection for films grown for 30 minutes at 400 and 450 °C, where the intensity of the former is several times greater than that of the latter. For a deposition time of 60 minutes, the intensity of the (004)/(200) planes for films deposited at 400 °C is greater than that for films deposited at 450 °C. Generally, the relative intensities of reflection from diffractograms show a striking similarity to the reference pattern suggesting preferential growth along the (112) plane.

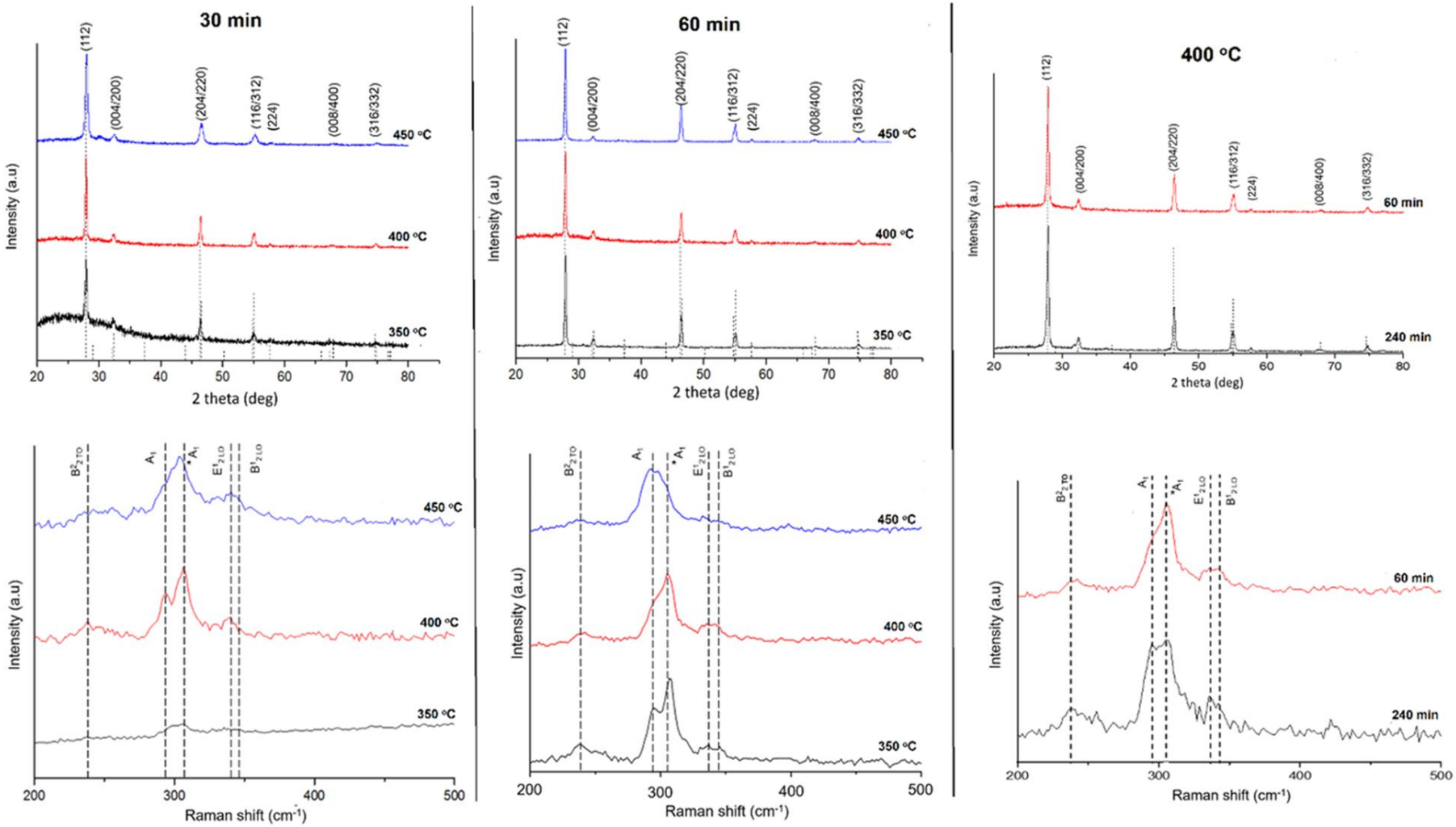

Figure 1. Normalized powder X-ray diffractograms with corresponding reference peak positions for CIS chalcopyrite (tetragonal structure, ICDD reference no. 00-027-0159)[22] and Raman spectra from films deposited at various temperatures and times.

Furthermore, at higher temperature there is marginal increase in crystallite size estimated from the Scherrer formula[23] for the (112) lattice plane reflection indicating improved film quality, the result of which may be fewer defects such as particle grain boundaries,[24] thereby influencing charge carrier density and mobility. Overall, the influence of temperature has implications for particle growth mechanisms as reflected in changes in the crystallite size, particle size and morphology.[25]

Though p-XRD data suggest that the films are phase pure without secondary binary phases, it cannot distinguish chalcopyrite (CH) and copper-gold (CA) type tetragonal structures, both of a face centred cubic chalcogen lattice, differing in copper and indium sites.[26] As such, Raman spectral data in Figure 1 confirm a mixed phase of CH and CA-type tetragonal structures since bands at 295 – 298 and 303 – 305 cm^{-1}, respectively related to the S^{2-} ion A_1 and $*A_1$ vibrational modes overlap to form a broad band.[25,27] The presence of the metastable CA-type structure is not unexpected for CIS since its formation energy is 2 meV higher than that of the CH-type structure.[28] Absence of modes at 266 and 475 cm^{-1} which are characteristic of copper and indium sulphide impurities further confirms high quality films. However, there is a slight dependence of CH and CA-type structures on deposition time and temperature, evaluated from the relative shift in peak maxima of A_1 and $*A_1$ modes. Accordingly, film microstructures seem to be of a higher fraction of CA-type ordering since peak maximum occurs at ~305 cm^{-1} for the $*A_1$ mode relative to a shoulder at ~295 cm^{-1} for the A_1 mode. However, for deposition at 400 and 450 °C for 240 minutes there instead is an A_1 mode maximum and $*A_1$ mode shoulder suggesting a higher fraction of CH-type ordering. The CA-type structure is more metastable at lower temperatures and likely to form first, and so higher temperatures and longer deposition times can facilitate thermally induced cation re-ordering to the more stable CH-type structure, an outcome that demonstrates some means of controlling film quality. Thus in this system, the kinetic, metastable product is the CA-type phase which gradually transforms into the thermodynamically stable CH-type phase with increased temperature.

Film morphology and composition

SEM micrographs of as-deposited thin films at respective temperatures are shown in Figure 2 and confirm different morphologies of well-compacted, highly crystalline microstructures with smooth facets. Films deposited at 350 °C consist of irregular faceted grains of sizes 0.2 – 0.5 μm whilst those deposited at 400 °C have larger grains of sizes 0.3 – 1.2 μm, some of which are irregular

pyramid-shaped. However, films deposited at 450 °C consist of a mixture of randomly oriented and distributed smooth-faceted microstructures including irregular faceted grains of 1 – 2 μm, pyramid-like grains of 1.2 – 1.5 μm as well as irregular microplates of length 1 – 5 μm and thickness 0.2 – 0.5 μm, stacked relatively normal to the substrate surface. Thus, it is important to note that the differences in morphology are likely attributed to variable growth mechanisms.

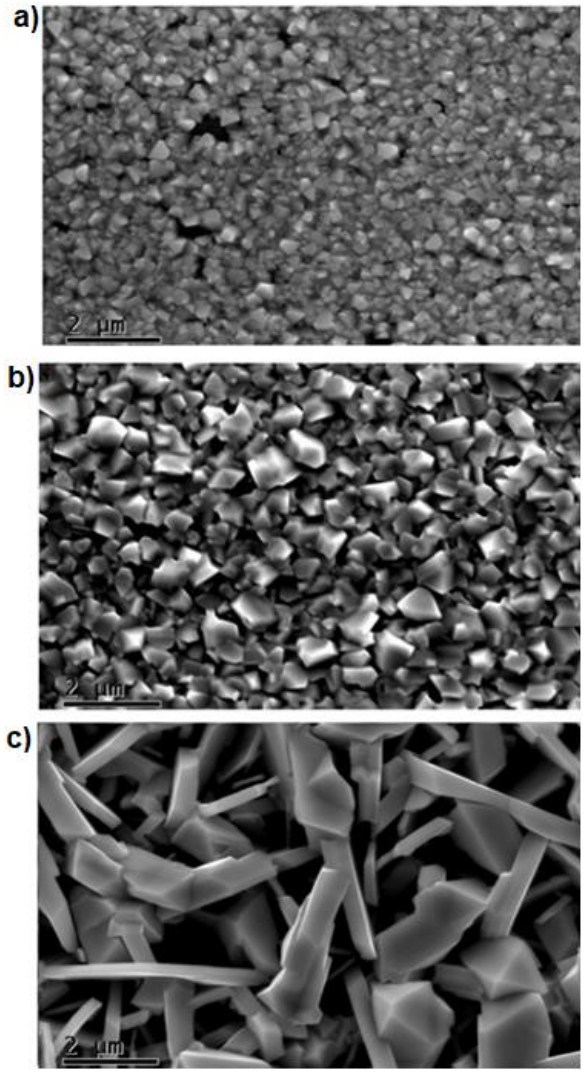

Figure 2. SEM images of CIS films deposited for 60 minutes at a) 350, b) 400 and c) 450 ^{o}C.

It is notable that a change in deposition mechanism from surface-reaction limited growth to mass-transport limited growth of monomer species is typically observed in chemical vapour deposition and as such the associated growth rate influenced by deposition temperature highlights the mechanism limiting film growth.[29-33] In this context, we suggest

that at lower deposition temperatures of 350 and 400 °C, there is rapid diffusion of precursor monomers across a narrow boundary layer to the substrate surface (i.e. surface-reaction limited growth) with high deposition rate of ions resulting in numerous nucleation sites growing at different rates. The slightly larger particles deposited at 400 ^{o}C compared to those at 350 ^{o}C suggest an inverse relationship of deposition rate with temperature. Overall, formation of irregular faceted microcrystals at these two temperatures is due to multidirectional growth along the preferred orientation (112) lattice plane from these numerous nucleation sites. However, a change in morphology at 450 °C may be due to limited diffusion of ions across a wider boundary layer during growth (i.e. mass-transport limited growth).[34-37] This results in a reduced number of small nucleation crystallites to which monomer ions are added along the (112) lattice plane influencing the growth of larger microstructures *via* coalescence of crystallites. Typically, a change in morphology is reflected in the intensity of the p-XRD reflections,[37] however a change in morphology at 450 °C does not deviate from the relative diffraction peak intensities of other samples which supports the preposition of coalescing crystallites which share a similar growth orientation as the emergent microstructure. We relate this to similar findings by Schlupp *et al.*[32] where Gd-doped films exhibited grain sizes of 10 nm from a surface-reaction limited growth regime at lower temperature but above 400 °C mass-transport limited growth induced agglomeration of crystallites into larger particles. Furthermore, the reflections from the minor lattice planes, (204/220) and (116/312) are most intense for films grown at 450 °C suggesting other growth orientations resulting in a change in particle morphology. Certainly, it is difficult to precisely determine the primary factors influencing the growth mechanism without a more systematic investigation involving synthetic variables and so, the influence of thermodynamic factors on the growth of larger particles at higher temperature cannot be disregarded. Therefore, an alternative mechanism for deposition at 450 ^{o}C could involve fewer larger crystallites nucleating, since smaller ones are thermodynamically less stable due to their higher formation energy (ΔG_f^{o}). Notwithstanding this, the resulting inhomogeneity of film morphology characterized by a variety of larger microstructures at 450 °C suggests competing growth mechanisms under suboptimal conditions for depositing thin films.

EDS elemental maps in Figure S1 ESI† display an even distribution of Cu, In and S elements irrespective of thin film. Atomic content confirm compositions of $Cu_{1.09}In_{1.22}S_{1.69}$, $Cu_{1.03}In_{1.03}S_{1.94}$ and $Cu_{0.95}In_{1.06}S_{1.99}$ for films deposited at temperatures of 350, 400 and 450 °C respectively (Table 1). Films deposited at 400 °C have stoichiometric metal content, whereas those deposited at 350 and 450 °C are copper-deficient. However, films synthesized at 400 °C are not only more stoichiometric but homogenous which shows the utility of AACVD for deposition of CIS thin films of desirable film quality. Furthermore, it has been reported that off-stoichiometry, specifically copper and sulphur deficiencies typically form the CA-type structure.[27,28,38] Here, the film compositions comport with Raman spectral data indicating CIS of both CH and CA-type structures. However, the CH content in films can be improved by manipulating precursor composition as demonstrated by Su *et al.*,[39] in which copper-rich polycrystalline films had a smaller CA-type domain size than stoichiometric epitaxial films evidenced from selected-area electron diffraction patterns of transmission electron microscopy. Also, Rudigier *et al.*[40] and Riedle *et al.*[41] independently confirmed that annealing at 475 °C under copper-rich conditions resulted in the CH phase with binary CuS impurities. These outcomes demonstrated that copper-rich conditions allowed for preferential formation of a predominantly CH structure without the CA-type phase. Invariably, it could also be assumed that off-stoichiometry is influenced by growth orientation of the (112) lattice plane and limited migration of atoms *via* grain boundaries. Notably, Eberhardt and co-workers[35] suggested that grain boundaries in stoichiometric polycrystalline CIS films facilitated surface segregation of excess Cu^{+} and S^{2-} ions as CuS_x phase, whereas easy diffusion routes did not exist in non-stoichiometric epitaxial CIS. Accordingly, under the growth conditions for our films, planar defects in larger particles facilitate some re-ordering of ions from the metastable CA-population of point defects and render off-stoichiometry, essentially copper and sulphur-deficient limiting maximal transformation of the CA-type to the CH structure. On this premise, it is possible that transformation into the preferred CH structure may depend on precursor composition, i.e., an excess of copper and sulphur with a delicate balance to prevent their segregation to the secondary CuS_x phase in copper-rich films. Though elemental composition influences the phase, it appears in our case that deposition temperature and by extension thermodynamic factors are influential in forming a primarily chalcopyrite material. Certainly, if composition is the prevailing factor, copper-deficient films deposited at 450 °C would have the lowest chalcopyrite content. However, it is more plausible to suggest that an optimal and delicate

balance between temperature and time (thermodynamic and kinetic factors) are required under conditions of sulphur annealing conditions, for example.

Optical properties

Charge carrier recombination *via* band gap defect states is a major contributor to low solar cell efficiency,[4] however, if controlled can effectively tune the photo-absorption. Therefore, the optical properties of thin films reported herein can be tuned since their composition, morphology and phase structures are dependent on AACVD experimental conditions.[7,41,42] Films deposited at various times and temperatures display variable near-infrared absorption as shown in Figure 3(i, iii) with estimated band gaps from Tauc plots between 1.32 and 1.42 eV, recorded in Table 1. Films deposited at 400 °C have a wider band gap (~1.42 eV) than those deposited at 350 °C (~1.38 eV), whereas films deposited at 450 °C have the narrowest band gap of ~1.32 eV. These variations could be related to microstructure size, morphology, composition and constituent native defects.[37,45,46] However, it is more plausible to suggest that they are attributed to the influence on the density of states of valence and conduction bands as a consequence of elemental composition.[8,45-48]

Table 1: Optical properties and elemental composition (derived from EDS) of CIS thin films.

Temperature/^{o}C	Band Gap, E_g/eV	Emission λ/nm	Elemental Content/%			Stoichiometry
			Cu^{+}	In^{3+}	S^{2-}	
350	1.38	~890 – 1087	27.2	30.5	42.3	$Cu_{1.09}In_{1.22}In_{1.69}$
400	1.42	~890 – 1087[a]	25.7	25.8	48.5	$Cu_{1.03}In_{1.03}S_{1.94}$
450	1.32	~890 – 1087[b]	23.7	26.6	49.7	$Cu_{0.95}In_{1.06}S_{1.99}$

[a]Most intense peak at 919 nm; [b]significant broadening of peak at 1059 nm.

As expected, there is no emission in the visible region but a series of inhomogeneous broad near-infrared bands between 890 and 1087 nm (1.40 and 1.14 eV) as shown in Figure 3(ii, iv), likely resulting from charge carrier recombination involving intrinsic defect states as reported for CIS and similar films prepared by other methods.[35,43,44] In particular, shallow donor levels associated with sulphur vacancies ($V_S^{\bullet\bullet}$) and indium interstitials ($In_i^{\bullet\bullet\bullet}$) have been implicated alongside deep donor electronic states of indium, copper antisities ($In_{Cu}^{\bullet\bullet}$) and shallow acceptor states of copper

vacancies (V_{Cu}').[43,49,50] Herein, the optical properties are not strongly dependent on band-to-band transitions as seen from the very weak emission at 890 nm (1.40 eV).

Based on the elemental composition determined from EDS data along with findings from other authors,[4,36,43,49,51] the proposed electronic transitions with their corresponding energy were evaluated from the emission spectra and summarized in Table 2. It has been reported that considerable sulphur deficiency of CIS is characterized by a high population of vacancies, $V_S^{\bullet\bullet}$ as donor states reported at 0.035 eV close to the conduction band minimum.[4] As such, the most intense emission at ~1.35 eV (918 nm) could be related to transition from these $V_S^{\bullet\bullet}$ donor states to the valence band or shallow acceptor states. Since donor – acceptor pairs (DAPs) are likely significant, transitions such as $V_S^{\bullet\bullet}$ to V_{Cu}' (954 nm; 1.30 eV), $In_i^{\bullet\bullet\bullet}$ to V_{Cu}' and/or valence band (969 – 1012 nm; 1.22 – 1.28 eV) and $In_{Cu}^{\bullet\bullet}$ to V_{Cu}' and/or valence band (1059 – 1087 nm; 1.22 – 1.28 eV) cannot be ruled out.

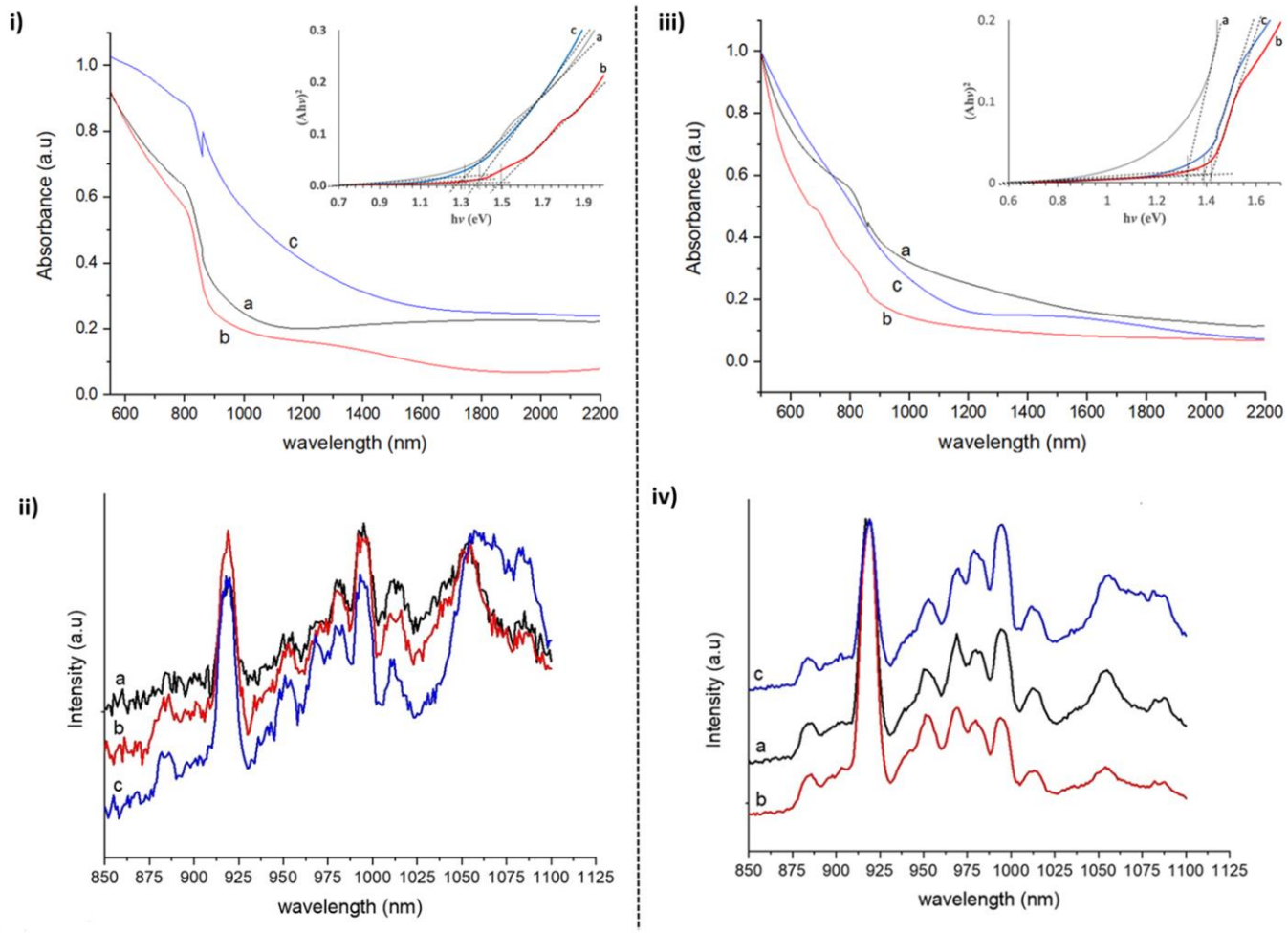

Figure 3. Normalised room temperature absorption vis-NIR (inset; Tauc plot) and photoluminescence spectra for films deposited for 30 mins (left) and 60 mins (right) at a) 350, b) 400 and c) 450 °C. Magnified Tauc plots included in Figure S2 ESI†.

Table 2: Summary of proposed electronic transitions with corresponding emission wavelength and energy for CIS films.

Emission		Transition
λ/nm	Energy/eV	
890	1.40	CB to VB
918	1.35	$V_S^{\bullet\bullet}$ to VB
954	1.30	$V_S^{\bullet\bullet}$ to V_{Cu}'
969 – 1012	1.22 – 1.28	$In_i^{\bullet\bullet\bullet}$ to V_{Cu}'/ VB
1059 – 1087	1.14 – 1.18	$In_{Cu}^{\bullet\bullet}$ to V_{Cu}'/ VB

B. Manganese, nickel and silver-doped CIS films

Evidently, the optimal AACVD conditions for depositing more stoichiometric, high quality, homogenous films are at 400 °C for 60 minutes, which seems suitable for attempted doping with varying mole fractions of Mn^{2+}, Ni^{2+} or Ag^{+} ions. Accordingly, EDS data (Table 3) confirm sulphur-deficient Mn-doped thin films with Cu/In = 1.14 and 0.88, respectively whilst p-XRD confirm tetragonal structure (Figure 4(i)) of irregular shaped microcrystals of ca. 0.2 – 0.5 μm, similar to undoped films (Figure 5(a)). Notably, vis-NIR absorption spectra (Figure 4(ii)) of films with Mn^{2+} added exhibit shoulders with slightly lower intensities than the undoped CIS, indicating a reduction in the density of energy states associated with this electronic transition possibly attributed to doping levels. However, it appears that the dopant content has no effect on tuning the band gaps (~1.41 eV) as shown from Tauc plots in Figure 4(iii) and recorded in Table 3.

On the other hand, CIS thin films with 1 and 2 % Ni^{2+} synthetically added show markedly different and tunable properties. Unlike undoped films, those with 1 % Ni^{2+} added consist of well-compacted, semi-crystalline irregular shaped microstructures of *ca.* 0.2 μm, whilst those with 2 % Ni^{2+} added have flake-like perforated microstructures up to 5 μm in width (Figure 5 (b)). However, overlapping Kα and Lα X-ray peaks associated with Cu^{2+} and Ni^{2+} ions rendered determination of the Ni^{2+} content from EDS ambiguous. Nonetheless, the data summarized in Table 3 and EDS elemental maps in Figure S3 ESI† indicate that homogenous film microstructures are sulphur-rich with Cu/In = 0.92 and 0.89, respectively. The p-XRD data in Figure 4(iv) confirm the CH structure, however a slight blue-shift of the (204) reflection at around $2\theta = 38°$ relative to that of the calculated tetragonal pattern is likely associated with the presence of domains of the CA-type phase.[52] Since the films maintain the same tetragonal structure, the change in morphology may be consistent with a change in composition as seen for undoped films. However, considering the red-shift in optical band gaps to 1.21 and 1.28 eV, respectively, relative to the undoped of 1.42 eV (Figure 4(v, vi)), it couldn't be established that these are associated with Cu/In ratio and an assumption about the nature and extent of defects states, even those associated with Ni^{2+} on the optical properties cannot be made in the absence of more probing electronic spectroscopy.

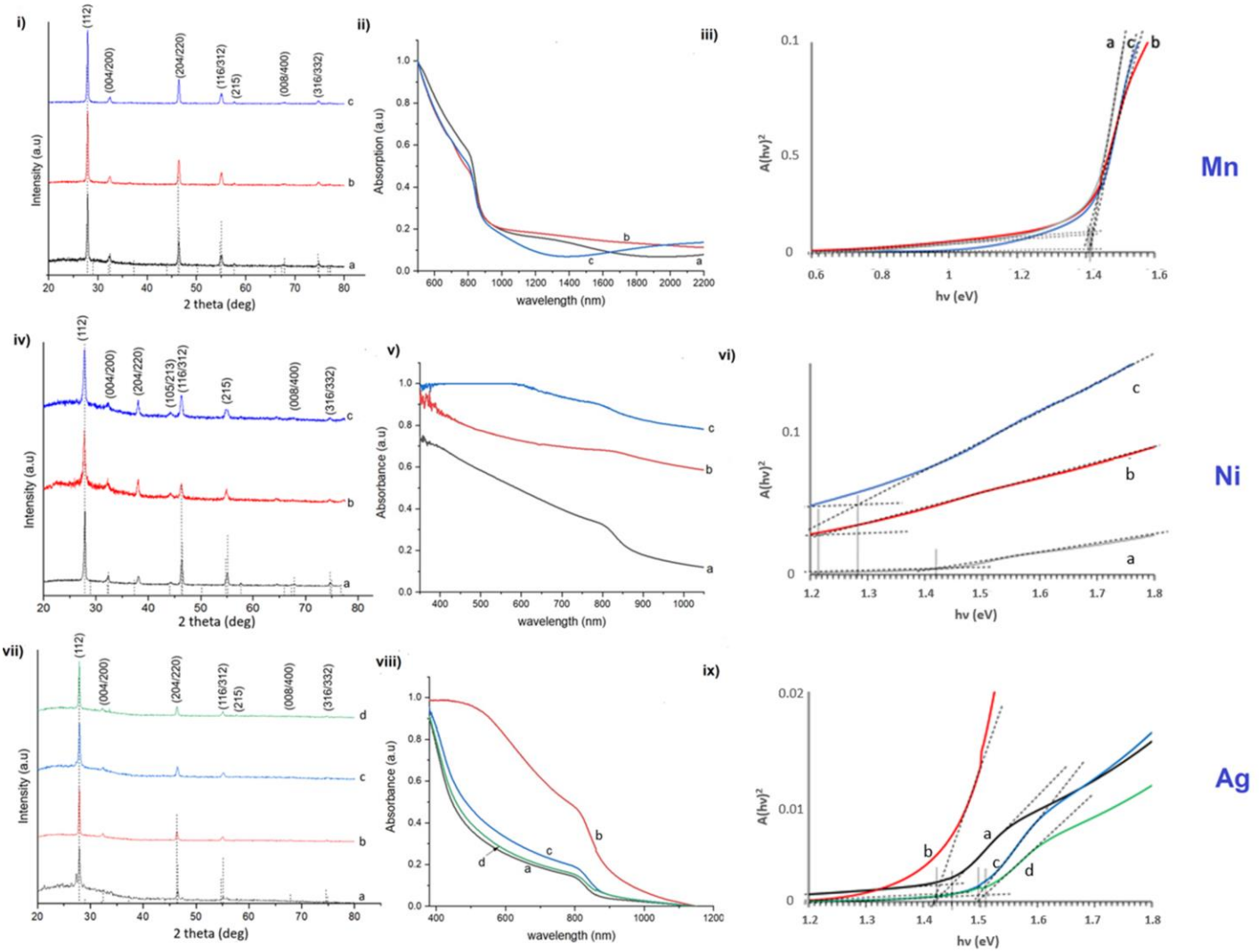

Figure 4. Normalized powder X-ray diffractograms with reference peak positions for CIS chalcopyrite (tetragonal structure, ICDD reference no. 00-027-0159)[22] and vis-NIR absorption spectra and Tauc plots (Figure S2 ESI†) for films of dopant additions: (i - iii) - Mn^{2+} ions a) 0, b) 1, c) 2 %; (iv - vi) - Ni^{2+} a) 0, b) 1, c) 2 %; and (vii - ix) - Ag^{+} a) 2.5, b) 5.0, c) 7.5, d) 12.0 %.

Table 3: EDS elemental composition and corresponding band gap values for Mn, Ni and Ag-doped CIS thin films.

Dopant amount added during synthesis/%		Band gap, E_g/ eV	Elemental content (%) and ratio					Stoichiometry
			Dopant	Cu^{+}	In^{3+}	S^{2-}	Cu^{+}/In^{3+}	
Mn^{2+}	0	1.42	-	25.7	25.8	48.5	1.00	$Cu_{1.03}In_{1.03}S_{0.97}$

	1	1.41	0.7	29.1	25.7	44.5	1.14	$Mn_{0.01}Cu_{1.17}In_{1.03}S_{0.89}$
	2	1.41	2.2	26.8	30.5	40.5	0.88	$Mn_{0.02}Cu_{1.07}In_{1.22}S_{0.81}$
	0	1.42	-	24.4	24.3	51.2	1.01	$Cu_{0.98}In_{0.97}S_{1.02}$
Ni^{2+}	1	1.21	0.1	22.6	24.7	52.6	0.92	$Ni_{0.001}Cu_{0.90}In_{0.98}S_{1.05}$
	2	1.28	0.0	22.8	25.6	51.6	0.89	$Ni_xCu_{0.91}In_{1.03}S_{1.03}$
	2.5	1.42	0.2	23.9	22.1	53.9	1.08	$Ag_{0.002}Cu_{0.95}In_{0.88}S_{2.16}$
			[1]1.6	23.8	23.4	52.2	1.02	$Ag_{0.016}Cu_{0.94}In_{0.94}S_{2.09}$
	5.0	1.45	0.8	23.7	25.5	50.1	0.93	$Ag_{0.008}Cu_{0.95}In_{1.02}S_{2.00}$
Ag^+	7.5	1.50	0.4	23.8	25.6	50.2	0.93	$Ag_{0.004}Cu_{0.95}In_{1.02}S_{2.00}$
	12.0	1.51	0.4	23.3	25.9	50.4	0.90	$Ag_{0.004}Cu_{0.93}In_{1.04}S_{2.02}$
			[2]0.5	34.4	23.2	41.9	1.48	$Ag_{0.005}Cu_{1.38}In_{0.93}S_{1.68}$

[1]Inside particle crater shown in [Figure 5(c)-2.5 %)]; [2]highly faceted grain shown in [Figure 5(c)-12.0 %)].

Films synthesized with 2.5 to 12.0 % Ag^+ added also possess a chalcopyrite structure as confirmed from the p-XRD data in Figure 4(vii). However, these show an additional peak at around $2\theta = 27°$ which is likely associated with domains of the CA phase since as previously reported, the CA-type structure shows a reflection that is slightly red-shifted relative to the (112) reflection of the CH structure.[52] The films which consist of irregular faceted grains with micro-indentations or craters consistently permeating their topography (Figure 5(c)), exhibit a slight blue-shift in band gap from 1.42 to 1.51 eV as shown in Figure 4(viii, ix). EDS data confirm an expected decrease in stoichiometric contributions from Cu^+ ions with Cu/In ratios of 1.08, 0.93, 0.93 and 0.90 for films of 2.5, 5.0, 7.5 and 12.0 % Ag^+ dopant additions, respectively. However, only a small fraction (0.2 to 0.8 %) of Ag^+ dopant was detected in the films. Nevertheless, the elemental data are useful in understanding aspects of the granular features of the films. For example, the micro-indentations of particles as shown in the first inset of Figure 5(c) have a much higher Ag^+ content than the collective Ag^+ content of the entire film, as recorded in Table 3. This suggests that the Ag^+ ion

dopant may have an important role in the development of indentations and the resultant particle morphology. Additionally, from EDS it is shown that the larger pyramidal, highly faceted grains magnified in the inset of films with 12.0 % Ag^{+} content (added) in Figure 5(c) are copper-rich (Cu/In = 1.48) and sulphur-poor in comparison to the slightly copper-poor content (Cu/In = 0.90) observed for the entire film. A copper-rich content in films has been reported to produce larger grains in comparison to more stoichiometric films[53,54] and so might be a likely reason for the larger grain size.

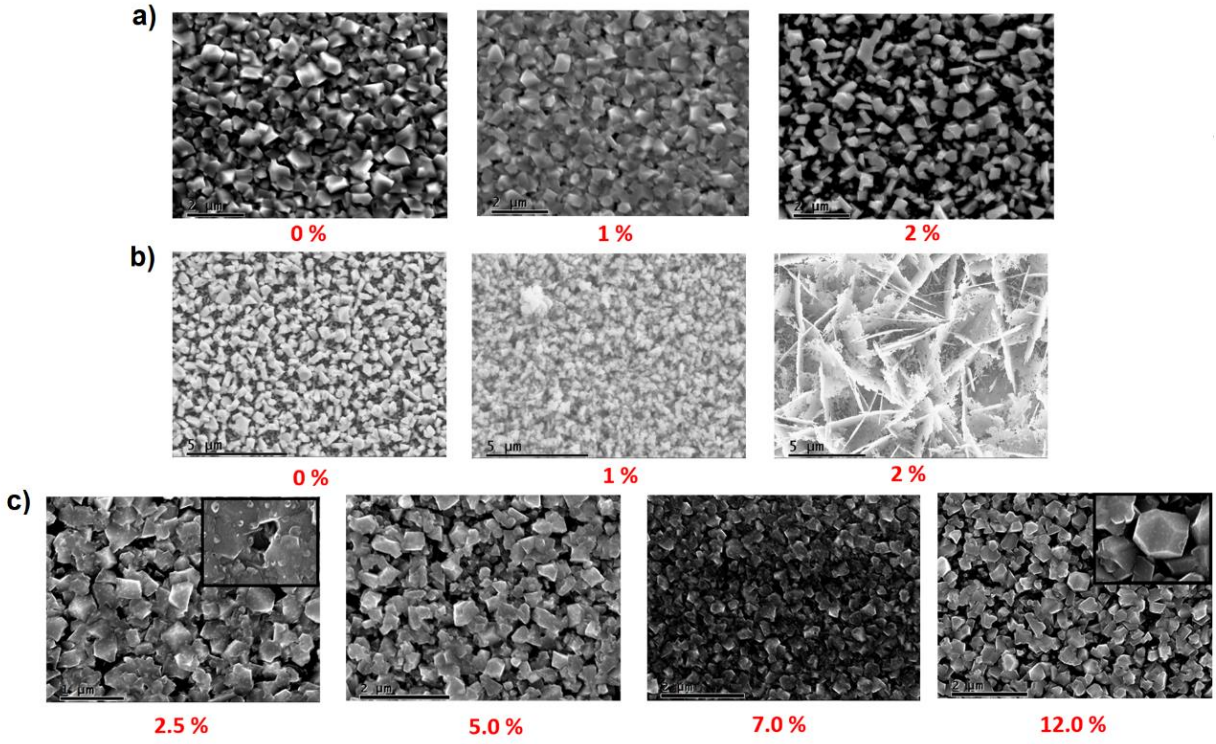

Figure 5. SEM images of doped CIS thin films with different dopant amounts added during synthesis; a) Mn^{2+}, b) Ni^{2+}, c) Ag^{+}.

Though SEM-EDS data provide some insight about grain morphology, the low percentage of Ag^{+} is puzzling especially since the dopant precursor was soluble in the solvent and available throughout the deposition period. Since a precise understanding of the basis of the very low concentrations of Ag^{+} isn't obvious, it is not unreasonable to suggest that this could be related to either (i) the smaller ion size of Ag^{+} relative to Cu^{+} and the energetics of lattice inclusion or (ii) the extent of mass transport across the deposition region and therefore possibly present on other poorly

deposited films. Notwithstanding the low Ag^{+} content, the slight blue-shift of band gap between 1.42 and 1.51 eV is possibly correlated to a decrease in Cu/In ratio. These preliminary outcomes suggest that a more systematic approach can be employed to tune the optical properties of doped CIS thin films using AACVD with an emphasis on intentional manipulation of composition for improved doping efficacy.

Conclusion

In this study, aerosol-assisted chemical vapor deposition is effectively employed to tune structure, composition, morphology and optical properties of undoped copper indium sulphide thin films as well as those doped with Mn^{2+}, Ni^{2+} and Ag^{+} ions. Under variable experimental conditions of deposition temperature and time, undoped CIS thin films consist of off-stoichiometric tetragonal (chalcopyrite and copper-gold-type) phase microcrystals. Data from p-XRD, Raman spectroscopy and SEM-EDS suggest a correlation of film structure, morphology and composition with deposition factors. Well-compacted and highly crystalline microstructures of variable morphology and predominantly chalcopyrite structure are obtained at 60 minutes of deposition and higher temperature of 450 ^{o}C. All films are slightly sulphur-deficient with more stoichiometric films deposited at 400 °C, whilst those deposited at 300 and 450 °C are copper-deficient. Near-infrared optical absorption of films shows some correlation of composition/structure with band gaps between 1.32 and 1.42 eV. Correspondingly, near-infrared emission suggests transitions implicated by donor – acceptor pairs involving deep or shallow states such as sulphur vacancies ($V_S^{\bullet\bullet}$) and indium-copper anti-sites ($In_{Cu}^{\bullet\bullet}$) as donors and copper vacancies ($V_{Cu}^{\prime}$) and indium interstitials ($In_i^{\bullet\bullet\bullet}$) as acceptors. Similarly, tetragonal phase microcrystals of thin films with Ni^{2+} and Ag^{+} dopants exhibit notably tunable morphology and near-infrared absorption whilst those with Mn^{2+} added show no obvious tunable properties. Based on these findings it can be envisaged that tunable optical properties of CIS can be achieved through varying experimental parameters, composition (copper content) and extrinsic doping *via* AACVD.

Experimental

Materials

Indium(III) diethyldithiocarbamate, $In(dedtc)_3$, copper(II) diethyldithiocarbamate, $Cu(dedtc)_2$, nickel(II) diethyldithiocarbamate and $Ni(dedtc)_2$ were prepared and purified according to a

literature method.[54] Silver(I) diethyldithiocarbamate, Ag(dedtc) was used as purchased from Aldrich. Mn(II) diethyldithiocarbamate, $Mn(dedtc)_2$ was unstable under synthetic conditions and manganese chloride tetrahydrate, $MnCl_2.4H_2O$ (Aldrich, 99.99 %) was instead used. Tetrahydrofuran, THF (Aldrich, ≥ 99.9 %) was used without further purification and acetone, methanol, ethanol and toluene dried using standard techniques. Quartz substrates were ultrasonically cleaned in purified ethanol and acetone, respectively.

Synthesis of Diethyldithiocarbamate Precursors of Cu(II), In(III) and Ni(II)

In a typical synthesis, stoichiometric amounts of respective metal salts, $InCl_3$, $CuCl_2$ and $NiCl_2.6H_20$, were dissolved in a minimum amount of distilled water, cooled in an ice bath and then added dropwise to a stoichiometric amount of $Nadedtc.3H_2O$, dissolved in 40 mL 50:50 mixture of methanol and water with constant stirring. $In(dedtc)_3$, $Cu(dedtc)_2$ and $Ni(dedtc)_2$ crystals were obtained by vacuum filtration, washed several times with methanol, recrystallized from toluene and left to dry.

$Cu(dedtc)_2$: Elemental analysis, found (%): C, 33.69; H, 5.73; N, 7.74; S, 35.74; Cu, 17.71. Calculated (%) for $C_{10}H_{20}CuN_2S_4$ (360.07 g/mol): C, 33.36; H, 5.60; N, 7.78; S, 35.62; Cu, 17.65. IR (ν_{max}, cm^{-1}): 2854-2961 (ν_s C-H), 1497 (ν_{as} C-N), 1274 (ν_{as} C-S), 988 (ν_s C-S).

$In(dedtc)_3$: Elemental analysis, found (%): C, 33.02; H, 5.53; N, 7.39; S, 34.24; In, 20.47. Calculated (%) for $C_{15}H_{30}InN_3S_6$ (559.63 g/mol): C, 32.21; H, 5.41; N, 7.51; S, 35.62; In, 20.53. IR (ν_{max}, cm^{-1}): 2864-2977 (ν_s C-H), 1499 (ν_{as} C-N), 1268 (ν_{as} C-S), 986 (ν_s C-S).

$Ni(dedtc)_2$: Elemental analysis, found (%): C, 34.11; H, 5.76; N, 7.84; S, 36.13; Ni, 16.54. Calculated (%) for $C_{10}H_{20}NiN_2S_4$ (360.10 g/mol): C, 33.81; H, 5.68; N, 7.81; S, 36.10; Ni, 16.52. IR (ν_{max}, cm^{-1}): 2853-2979 (ν_s C-H), 1500 (ν_{as} C-N), 1274 (ν_{as} C-S), 998 (ν_s C-S).

Thin film deposition

AACVD was performed in a quartz tube embedded in a horizontal bed cold-walled tubular (17 cm x 6 cm) furnace. $Cu(dedtc)_2$ (0.15 mmol) and $In(dedtc)_3$ (0.15 mmol) in 20 mL THF were aerosolized by a piezoelectric modulator and transported *via* an argon flow of 200 sccm to the reactor. Subsequent deposition and growth onto 2 × 1 cm quartz substrates occurred at temperatures of 350, 400 and 450 ℃ for 30, 60 and 240 minutes, yielding dark brown uniform films located in

the centre of the reactor tube. For doping experiments, 1 and 2 mol % $Ni(dedtc)_2$ or $MnCl_2.4H_2O$ and 2.5 – 12.0 % Ag(dedtc) substituted $Cu(dedtc)_2$.

Precursor decomposition

Elemental analysis (Table S2 ESI†) of precursors $Cu(dedtc)_2$, $In(dedtc)_3$, $Ni(dedtc)_2$ and Ag(dedtc) confirm their high purity. Thermograms in Figure S4 ESI† show clean, one step decomposition; comparable calculated and experimental % mass residues suggest Cu_2S, In_2S_3, NiS and Ag_2S were formed from respective metal chalcogenide precursors recorded in Table S3 ESI†. Similar decomposition ranges suggest that precursors are suitable for deposition of undoped and doped $CuInS_2$ thin films from Cu_2S, In_2S_3, NiS and Ag_2S monomers between 350 and 450 °C *via* AACVD.

Measurements

X-ray diffractograms of as-synthesized thin films were recorded using a Bruker D8 Advance X-ray diffractometer with filtered Cu-Kα radiation (λ = 0.15406 nm) within a 2θ range 20 to 80° and step size 0.02°/second for 2½ hours operating at 40 mA and 20 kV. Diffractograms were auto-indexed (representative data in Table S4 ESI†) using the X′Pert HighScore software. For some samples, a Rigaku Ultima III diffractometer with the same scan parameters, was used instead. Raman spectroscopy was carried out using a Renishaw RM System 1000 Mk1 Raman spectrometer with Modu-Laser Aries 163 514/25 argon-ion 514 nm 25 mW laser. Spectra were recorded at 0.277 mW laser power with 50× objective lens within the range 26 – 1000 cm^{-1}. Absorption spectra were recorded with a Perkin Elmer Lambda 1050 UV/vis/NIR spectrometer within the range 500 – 2200 nm. An Edinburgh Instruments FLS920 spectrometer was used to record emission spectra within the region 815 – 1200 nm, exciting at 790 nm. Microscopic images of thin film surface were captured using a Phillips XL 30 field emission gun (FEG) scanning electron microscope with electron beam accelerating voltage of 10 kV and working distance of 10 mm, and energy dispersive spectroscopic (EDS) data recorded to deduce elemental composition with electron beam accelerating voltage of 20 kV. For some samples a JEOL-JSM 7600F SEM with Oxford instruments EDS detector using similar collection parameters, was used instead. Thermogravimetric analyses (TGA) of molecular precursors were done between 25 and 600 °C in nitrogen on a Mettler Toledo TGA/DSC1 instrument and elemental analyses (EA) for carbon,

hydrogen, nitrogen, copper, indium, nickel and sulphur were carried out using a Flash 2000 elemental analyzer. The infrared spectra (IR) of precursors were collected from 650 to 4000 cm^{-1} at resolution of 2 cm^{-1} using a Perkin Elmer Thermo Scientific ID5-ATR spectrometer.

Conflicts of interest

There are no conflicts to declare.

CRediT author statement

Shanna-Kay Ming: investigation, data curation, draft preparation, writing-reviewing, editing. Richard Taylor: principal investigator, writing-reviewing, editing, supervision, visualization, conceptualization. Paul O'Brien: co-supervision, resources. Paul McNaughter: writing-reviewing, editing, co-supervision. David Lewis: writing-reviewing, editing, supervision.

Acknowledgements

The authors extend thanks to the Department of Chemistry, School for Graduate Studies and Research as well as the Office of the Dean, Faculty of Science and Technology, University of the West Indies, St. Augustine campus for financial assistance. This research was partly made possible with a TWAS Research Grant (UNESCO FR: 324026725) and Brookhaven National Laboratory (proposal numbers: 36576, 38881).

Notes and references

1. H. Zhong, Y. Zhou, M. Ye, Y. He, J. Ye, C. Yang and Y. Li, Chem. Mater., 2008, **20**, 6434-43.
2. S.N. Malik, A.Q. Malik, R.F. Mehmood, G. Murtaza, Y.G. Alghamdid and M.A. Malik., New J. Chem., 2015, **39**, 4047-54.
3. R. Klenk, J. Klaer, C. Köble, R. Mainz, S. Merdes and H. Rodriguez-Alvarez, Sol. Energy Mater. Sol. Cells, 2011, **95**, 1441-5.
4. J. Hofhuis, J. Schoonman and A. Goossens, J. Phys. Chem. C, 2008, **112**, 15052-9.
5. C. Coughlan, M. Ibáñez, O. Dobrozhan, A. Singh, A. Cabot and K.M. Ryan, Chem. Rev., 2017, **117**, 5865-6109.
6. M.A. Majeed Khan, S. Kumar and M.S. AlSalhi, Mater. Res. Bull., 2013, **48**, 4277-82.

7. M. Krunks, O. Bijakina, T. Varema, V. Mikli and E. Mellikov, Thin Solid Films, 1999, **338**, 125-30.
8. B. Chen, H. Zhong, W. Zhang, Z. Tan, Y. Li, C. Yu, T. Zhai, Y. Bando, S. Yang and B. Zou, Adv. Funct. Mater., 2012, **22**, 2081-8.
9. G. Zaiats, S. Kinge and P.V. Kamat, J. Phys. Chem. C, 2016, 120, 10641-6.
10. J. Tamil Illakkiya, P. Usha Rajalakshmi and R. Oommen, Mater. Sci. Semicond. Process., 2016, **49**, 84-91.
11. D. Abou-Ras, S. Wagner, B.J. Stanbery, H.-W. Schock, R. Scheer, L. Stolt, S. Siebentritt, D. Lincot, C. Eberspacher, K. Kushiya and A.N. Tiwari, Thin Solid Films, 2017, **633**, 2-12.
12. P.D. Matthews, P.D. McNaughter, D.J. Lewis and P. O'Brien, Chem. Sci., 2017, **8**, 4177-87.
13. C. Manhendran and N. Suriyanarayanan, Optik., 2013, **124**, 5089-94.
14. S.D. Ponja, S. Sathasivam, I.P. Parkin and C.J. Carmalt, RSC Adv., 2014, 4, 49723-8.
15. A.C. Jones and M.L. Hitchman, Chemical Vapour Deposition: Precursors, Processes and Applications, ed. A.C. Jones and M.L. Hitchman, Royal Society of Chemistry, Cambridge, 2009, chapter 1, pp 1-36.
16. P. Marchand, I.A. Hassan, I.P. Parkin and C.J. Carmalt, Dalton Trans., 2013, **42**, 9406-22.
17. S. Basharat, C.J. Carmalt, R. Binions, R. Palgrave and I.P. Parkin, Dalton Trans., 2008, **5**, 591-5.
18. A. Hepp, J. McNatt, J. Dickman, M. Jin, K. Banger, C. Kelly, A. Aquino-González and A. Rockett, presented in part at the 4th International Energy Conversion Engineering Conference (IECEC), San Diego, California, June 26-29, 2006.
19. M. Afzaal, D. Crouch, P. O'Brien, J.-H. Park, MRS Proceedings, 2001, **692**, H6.8.1.
20. R. Nomura, Y. Sekl and H. Matsuda, J. Mater. Chem., 1992, **2**, 765-6.
21. S.S. Lee, K.W. Seo, J.P. Park, S.K. Kim and I.-W. Shim, Inorg. Chem., 2007, **46**, 1013-7.
22. A. Katerski, E. Kärber, I.O. Acik, L. Dolgov, A. Mere, I. Sildos, V. Mikli and M. Krunks, Nanoscale Res. Lett., 2014, **9**, 494-99.
23. Y. Zhiqiang, Z. Yu, Z. Mixue, L. Jun and W. Aixiang., J. Mater. Sci.: Mater. Electron., 2013, **24**, 5055-60.
24. E. Garskaite, G.-T. Pan, T.C.K. Yang, S.-T. Huang and A. Kareiva, Sol. Energy, 2012, **86**, 2584-91.
25. J.I. Langford and A.J.C. Wilson., J. Appl. Crystallogr., 1978, **11**, 102-13.

26. P. Prabukanthan, R. Lakshmi, G. Harichandran and T. Tatarchuk, New J. Chem., 2018, **42**, 11642-52.
27. J. Álvarez-García, B. Barcones, A. Pérez-Rodríguez, A. Romano-Rodríguez, J.R. Morante, A. Janotti, S.-H. Wei and R. Scheer, Phys. Rev. B., 2005, **71**, 1-9.
28. C. Stephan, Structural Trends in Off Stoichiometric Chalcopyrite Type Compound Semiconductors, Freie Universität Berlin, Germany, 2011.
29. T. Nabatame, M. Hiratani, M. Kadoshima, Y. Shimamoto, Y. Matsui, Y. Ohji, I. Asano, T. Fujiwara and T. Suzuki, Jpn. J. Appl. Phys., 2000, **39**, L1188.
30. C.R. Kleijn, R. Dorsman, K.J. Kuijlaars, M. Okkerse and H. van Santen, J. Cryst. Growth, 2007, **303**, 362-380.
31. D.-X. Yea, S. Pimanpanga, C. Jezewskib, F. Tanga, J.J. Senkevicha, G.-C. Wanga and T.-M. Lu, Thin Solid Films, 2005, **485**, 95-100.
32. M.V.F. Schlupp, M. Prestat, J. Martynczuk, J.L.M. Rupp, A. Bieberle-Hütter and L.J. Gauckler, J. Power Sources, 2012, **202**, 47-55.
33. R.N. Ghoshtagore, J. Electrochem. Soc., 1978, **125**, 110.
34. F.M. Courtel, A. Hammami, R. Imbeault, G. Hersant, R.W. Paynter, B. Marsan and M. Morin, Chem. Mater., 2010, **22**, 3752-61.
35. J. Eberhardt, J. Cieslak, H. Metzner, T. Hahn, R. Goldhahn, F. Hudert, J. Kräußlich, U. Kaiser, A. Chuvilin, U. Reislöhner and W. Witthuhn, Thin Solid Films, 2009, **517**, 2248-51.
36. C.V. Kelly, M.H.C. Jin, K.K. Banger, J.S. McNatt, J.E. Dickman, A.F. Hepp., Mater. Sci. Eng. B., 2005, **116**, 403-8.
37. M.H.C. Jin, K.K. Banger, J.D. Harris and A.F. Hepp, Mater. Sci. Eng. B., 2005, **116**, 395-401.
38. H.O. Pierson, Handbook of Chemical Vapour Deposition: Principles, Technology, and Applications, Noyes Publications/Williams Andrew Publishing, Norwich, New York, 1999.
39. D.S. Su, W. Neumann and M. Giersig, Thin Solid Films, 2000, **361-362**, 218-22.
40. E. Rudigier, T. Enzenhofe and R. Scheer, Thin Solid Films, 2005, **480-481**, 327-31.
41. T. Riedle, Raman Spectroscopy for the Analysis of Thin $CuInS_2$ Films, Technische Universität Berlin, Germany, 2002.
42. E. Rudigier, Phase Transformations and Crystalline Quality of $CuInS_2$ Thin Films, University of Marburg, Germany, 2004.

43. S. Chen, G. Carraro, D. Barreca, A. Sapelkin, W. Chen, X. Huang, Q. Cheng, F. Zhange and R. Binions, J. Mater. Chem. A, 2015, **3**, 13039-49.
44. A. Goossens and J. Hofhuis, Nanotechnology, 2008, **19**, 424018.
45. M. Nanu, F. Boulch, J. Schoonman and A. Goossens, J. Appl. Phys., 2005, **87**, 242103.
46. J.E. Jaffe and A. Zunger, Phys. Rev. B, 1983, **28**, 5822-47.
47. C. Yang, M. Qin, Y. Wang, D. Wan, F. Huang and J. Lin, Sci. Rep., 2013, **3**, 1286.
48. A. Soni, V. Gupta, C.M. Arora, A. Dashora and B.L. Ahuja, Sol. Energy, 2010, **84**, 1481-9.
49. B. Chen, H. Zhong, W. Zhang, Z. Tan, Y. Li, C. Yu, Z. Tianyou, Y. Bando, S. Yang and B. Zou, Adv. Funct. Mater., 2012, **22**, 2081-8.
50. A.D.P. Leach, X. Shen, A. Faust, M.C. Cleveland, A.D. La Croix, U. Banin, S. Pantelides and J. Macdonald, J. Phys. Chem. C, 2016, **120**, 5207-12.
51. J.S. Park, S. Kim, Z. Xie and A. Walsh, Nat. Rev. Mater., 2018, **3**, 194-210.
52. D. Delmonte, F. Mezzadri, G. Spaggiari, S. Rampino, F. Pattini, D. Bersani and E. Gilioli., Inorg. Chem., 2020, **59** (16), 11670-11675.
53. D. Perniu, S. Vouwzee, A. Duta and J. Schoonman, J. Optoelectron. Adv. Mater., 2007, **9**, 1568-71.
54. A. Khare, A.W. Wills, L.M. Ammerman, D.J. Norris and E.S. Aydil, Chem. Commun., 2011, 47, 11721-3.